STEADY STREAMING AROUND A SPHERICAL DROP DISPLACED FROM THE VELOCITY ANTINODE IN AN ACOUSTIC LEVITATION FIELD

by A. Y. REDNIKOV, HONG ZHAO, S. S. SADHAL†

(*Aerospace & Mechanical Engineering, University of Southern California, Los Angeles*, CA 90089-1453, *USA*)

and E. H. TRINH

(*NASA Headquarters, Code UG*, 300 *E Street SW, Washington*, DC 20546, *USA*)

[Received 4 October 2004. Revise 28 April 2006]

Summary

The steady (acoustic) streaming associated with a spherical drop displaced from the velocity antinode of a standing wave is studied. The ratio of the particle size to the acoustic wavelength is treated as small but non-zero, and the solution is developed in the form of a two-term expansion in terms of the corresponding smallness parameter. The drop viscosity is assumed to be much higher than that of the surrounding fluid, which is the case for a drop in a gas medium. There are essentially three distinct regions where the steady streaming flow is analysed: inside the drop (internal circulation), in the Stokes shear-wave layer at the surface on the gas side, and the gas outside the Stokes layer (the outer streaming region). Solutions for the internal circulation and the outer streaming are obtained in the limit of small Reynolds number.

Despite the gas-to-liquid viscosity ratio being small, the outer streaming may be dramatically affected by the fact that the sphere is liquid as opposed to solid. The parameter that measures the effect of liquidity is essentially the viscosity ratio divided by the relative (to the particle size) thickness of the Stokes layer. The case of a solid sphere is recovered by letting this parameter go to zero.

1. Introduction

Acoustic levitation is now in frequent use as an advanced technology for experiments in containerless processing. For such systems, the acoustic field provides the radiation pressure necessary to levitate a liquid drop in a gravitational field. The studies relating to the radiation pressure on disks and spheres were carried out as early as the 1930s by King (**1**, **2**). Subsequent investigations on the radiation force have been conducted for both drops and bubbles by many researchers (such as Apfel (**3**), Asaki and Marston (**4**), Eller (**5**), Lee and Wang (**6**), Wu and Du (**7**), Yosioka and Kawasima (**8**)).

Under microgravity conditions, acoustic fields can be used to control, position, and stabilize particles. In relation to this application, experimental work has been conducted by Trinh (**9**, **10**). In addition, there are analytical studies such as that by Lee and Wang (**11**) as well as Yarin *et al.* (**12**). Lee and Wang (**11**) considered an oscillating sphere slightly displaced from the antinode of a

†⟨sadhal@usc.edu⟩

Q. Jl Mech. Appl. Math, Vol. 59. No. 3 © The author 2006. Published by Oxford University Press;

Advance Access publication 9 June 2006. doi:10.1093/qjmam/hbl007

standing wave for the frequency parameter (defined below) $|M| \gg 1$. In their analysis, the Stokes layer is accounted for by allowing a tangential slip velocity on the surface of the sphere. The flow field for the displaced sphere is seen to be asymmetric about the equatorial plane of the sphere. This asymmetry is attributed to the asymmetric velocity distribution around the particle as a consequence of the compressibility of the oscillating flow.

With low gravity, liquid drops are generally undistorted and tend to be spherical in shape. Even with ground-based studies, the distortion of small liquid drops is often negligible and we may assume them to be spherical in shape. Drops larger than a few millimetres tend to deform into spheroidal shapes. The case of a highly distorted non-spherical drop has been numerically studied by Yarin, Pfaffenlehner and Tropea (**13**). Among the many results, they provide a relationship between the aspect ratio of the deformed drop and the sound pressure level. This is found to have good agreement with measurements. Also, quite recently, Rednikov and Sadhal (**14**) gave the analytical solution for a solid spheroid placed at the velocity antinode. They showed that although topologically the streaming around an oblate spheroid is quite similar to that for a sphere, the streaming intensity grows appreciably with decreasing minor radius. Additionally, the zone of most intense streaming shrinks and localizes to the vicinity of the equator.

There is fundamental interest in the streaming phenomenon that represents the non-zero time-averaged mean of a fluctuating flow. This is often the result of the nonlinear interaction of an oscillatory flow with a boundary. Some of the earliest works go back many decades (see, for example, Schlichting (**15**)) and perhaps even to as early as 1883 (Lord Rayleigh (**16**)). There are a few reviews of acoustic and other oscillatory-type streaming in the literature (**17** to **20**), as well as several applications to cylinders and spheres (**21** to **24**). Much of the earlier theoretical activity relevant to streaming about particles has been focused on solid spheres (Gopinath (**25**, **26**), Riley (**21**)), and there has been little investigation on the effect of the boundary-layer interaction with a fluid particle. The problem of streaming about an oscillating bubble has been studied by Davidson and Riley (**27**), and by Longuet-Higgins (**28**) who also included radial pulsations. Zhao, Sadhal and Trinh (**29**) examined the streaming about a high-viscosity liquid drop placed at the velocity antinode of a standing wave in a gaseous medium. One of their interesting results was the cessation of recirculation in the Stokes layer for certain ranges relating the frequency parameter and the liquid-to-gas viscosity ratio.

In the present study, we develop the flow field dealing with a liquid sphere in a gas medium displaced between the velocity node and the antinode in acoustic levitation. The analysis is carried out for a high-frequency standing acoustic wave which is used to levitate particles in Earth gravity or to stabilize particles in low-gravity situations. The drop is considered to have sufficient mass so that it occupies a stable position in the acoustic field and it does not experience significant body oscillations. A perturbation procedure based on small-amplitude and high-frequency assumptions is employed to derive the flow fields when particles are placed in the acoustic field. We choose axially symmetric spherical polar coordinates (r, θ) with the origin at the centre of the sphere. The z-axis passes through the centre of the sphere and points along the direction of vibration, and $z = 0$ represents the velocity antinode closest to the sphere, while $z = z_0$ is the centre of the sphere. The following dimensionless parameters are used:

$$M^2 = \omega a^2/\nu \gg 1, \quad \varepsilon = \frac{U_\infty}{\omega a} \ll 1, \quad \bar{k} = ka \quad \text{and} \quad R_s = \varepsilon^2 M^2 \ll 1,$$

where U_∞ is the velocity amplitude of the standing wave, ω is the frequency, ν is the kinematic viscosity of the gas medium, a is the drop radius, $k = \omega/c$ is the acoustic wavenumber, M is the

frequency parameter, ε is the amplitude parameter, which is actually the reciprocal of the Strouhal number. The high-frequency and small-amplitude case corresponds to $M \gg 1$ and $\varepsilon \ll 1$, respectively. We assume that the particle size is much smaller than the acoustic wavelength, that is, $\bar{k} \ll 1$, furthermore, R_s, the expected value of the Reynolds number for the resulting steady streaming (the streaming Reynolds number (**21**)), is also assumed to be small.

The flow parameters are scaled as follows:

$$\boldsymbol{u} = \frac{\boldsymbol{u}^*}{U_\infty}, \quad \psi = \frac{\psi^*}{U_\infty a^2}, \quad r = \frac{r^*}{a}, \quad z = \frac{z^*}{a}, \quad \varphi = \frac{\varphi^*}{U_\infty a},$$

$$t = \omega t^*, \quad p = \frac{p^*}{\rho_c^* U_\infty \omega a}, \quad \text{and} \quad \rho = \frac{\rho^* c^2}{\rho_c^* U_\infty \omega a},$$

where ρ_c^* is the unperturbed medium density, c is the speed of sound, ρ^* is the density perturbation due to the acoustic wave, and p^* is the acoustic pressure. The flow field will be described by the stream function ψ^* and the velocity potential φ^*. The asterisks denote dimensional variables while the dimensionless variables are without asterisks (although dimensional constants do not have asterisks). The dimensionless continuity and momentum equations may be written as

$$\bar{k}^2 \frac{\partial \rho}{\partial t} + \boldsymbol{\nabla}\cdot\boldsymbol{u} + \varepsilon \bar{k}^2 \boldsymbol{\nabla}\cdot(\rho \boldsymbol{u}) = 0 \tag{1.1}$$

and

$$(1 + \rho\varepsilon\bar{k}^2)\frac{\partial \boldsymbol{u}}{\partial t} + \varepsilon(1 + \rho\varepsilon\bar{k}^2)\boldsymbol{u}\cdot\boldsymbol{\nabla}\,\boldsymbol{u} = -\boldsymbol{\nabla}\, p + \frac{1}{M^2}\nabla^2 \boldsymbol{u}, \tag{1.2}$$

respectively. By using the adiabatic relation $\rho^* = p^*/c^2$ with c as the speed of sound, the dimensionless acoustic pressure and density can be shown to be equal for $\gamma = c_p/c_v \simeq 1$, that is,

$$p = \rho \tag{1.3}$$

to leading order.

A particle levitated in a gravity field would position itself between the velocity node and the antinode. To consider such a problem, we expand the standing-wave velocity u_z^* such that

$$\begin{aligned} u_z^* &= U_\infty \cos(kz^*)e^{i\omega t^*} = U_\infty \cos(\bar{k}z)e^{it} \\ &= U_\infty[\cos \bar{k}z_0 - \bar{k}(z - z_0)\sin \bar{k}z_0 + O(\bar{k}^2(z - z_0)^2)]e^{it} \end{aligned} \tag{1.4}$$

represents the local velocity in the neighbourhood of the sphere centred at $(z = z_0)$. As mentioned earlier, z_0 is the dimensionless displacement of the centre of the sphere from the velocity antinode. The first term in the expanded version of equation (1.4) is just the far-field velocity for the situation when the sphere is at velocity antinode of a standing wave, and the second term is the far-field velocity for the case when the sphere is positioned at the node. The cases $\bar{k}z_0 = 0$ and $\bar{k}z_0 = \frac{1}{2}\pi$ would correspond to cases of a sphere placed at the velocity antinode and node, respectively. The displaced sphere problem is a combination of Riley's (**21**) problem and the problem discussed in the paper by Zhao, Sadhal and Trinh (**30**), together with additional nonlinear terms.

While the fluid within the Stokes layer near the surface of the sphere has vorticity to meet the continuity conditions on the interface, the flow outside the layer behaves irrotationally as in a sound field. This outer flow field can therefore be expressed as a velocity potential,

$$\boldsymbol{u} = \boldsymbol{\nabla}\varphi. \tag{1.5}$$

The dimensionless far-field potential function, corresponding to equation (1.4), takes the form

$$\varphi_\infty = \left[\frac{1}{\bar{k}}\sin\bar{k}z_0 + (z-z_0)\cos\bar{k}z_0 - \tfrac{1}{2}\bar{k}(z-z_0)^2\sin\bar{k}z_0 + O\left(\bar{k}^2\right)\right]e^{it}$$
$$= \left[\frac{1}{\bar{k}}\sin(\bar{k}z_0) + r\cos(\bar{k}z_0)P_1(\bar{\mu}) - \tfrac{1}{6}\bar{k}r^2\sin(\bar{k}z_0)\right.$$
$$\left. - \tfrac{1}{3}\bar{k}r^2\sin(\bar{k}z_0)P_2(\bar{\mu}) + O\left(\bar{k}^2\right)\right]e^{it}, \tag{1.6}$$

where $P_n(\bar{\mu})$ denotes Legendre polynomials, and $\bar{\mu} = \cos\theta$. With the spherical coordinate system centred at $z = z_0$, it should be noted that $z - z_0 = r\bar{\mu}$. From momentum equation (1.2), we have

$$\frac{\partial \boldsymbol{u}_\infty}{\partial t} = -\boldsymbol{\nabla} p_\infty, \tag{1.7}$$

and using equation (1.5) we obtain

$$p_\infty = \rho_\infty = -i\left[\frac{1}{\bar{k}}\sin(\bar{k}z_0) + r\cos(\bar{k}z_0)P_1(\bar{\mu})\right.$$
$$\left. - \tfrac{1}{6}\bar{k}r^2\sin(\bar{k}z_0) - \tfrac{1}{3}\bar{k}r^2\sin(\bar{k}z_0)P_2(\bar{\mu})\right]e^{it}, \tag{1.8}$$

where the real part applies.

2. Solution

In this section, we analyse the flow field by the singular perturbation method using $\varepsilon = U_\infty/(\omega a)$ as a small parameter. In the present analysis, parameters with ($\hat{}$) represent properties of liquid inside the drop, and parameters without ($\hat{}$) correspond to the gas region outside the drop.

By applying the perturbation method, we expand the velocity, acoustic pressure and density outside the boundary layer in powers of ε as follows:

$$\boldsymbol{u} = \boldsymbol{u}_0 + \varepsilon\boldsymbol{u}_1 + O(\varepsilon^2), \tag{2.1}$$

$$p = p_0 + \varepsilon p_1 + O(\varepsilon^2), \tag{2.2}$$

and

$$\rho = \rho_0 + \varepsilon\rho_1 + O(\varepsilon^2). \tag{2.3}$$

These expansions are substituted into equations (1.1) and (1.2) to form a hierarchy of equations in orders of ε. We treat here the leading-order ($O(1)$) and $O(\varepsilon)$ terms.

2.1 *Leading-order solutions*

2.1.1 *Outer region.* From the continuity equation (1.1), the leading-order velocity satisfies

$$\bar{k}^2\frac{\partial\rho_0}{\partial t} + \boldsymbol{\nabla}\cdot\boldsymbol{u}_0 = 0. \tag{2.4}$$

From the momentum equation (1.2), we find that

$$\frac{\partial \boldsymbol{u}_0}{\partial t} = -\boldsymbol{\nabla} p_0, \tag{2.5}$$

which indicates that the leading-order outer flow behaves irrotationally. Thus, we can introduce the potential function φ_0, such that

$$\boldsymbol{u}_0 = \boldsymbol{\nabla}\varphi_0. \tag{2.6}$$

The use of (2.4) and (1.3) in (2.5) results in the standard wave equation,

$$\bar{k}^2 \frac{\partial^2 \rho_0}{\partial t^2} = \nabla^2 \rho_0 \quad \text{or} \quad \bar{k}^2 \frac{\partial^2 \varphi_0}{\partial t^2} = \nabla^2 \varphi_0. \tag{2.7}$$

Upon examining the far-field behaviour of ρ given by equation (1.8), we see that for small $\bar{k}$, the dominant term is $-i\,(1/\bar{k})\sin(\bar{k}z_0)e^{it}$. Therefore, maintaining the same order for ρ_0, and using (2.6), the continuity equation (2.4) becomes

$$\bar{k}\sin(\bar{k}z_0)e^{it} + \nabla^2\varphi_0 = 0. \tag{2.8}$$

The solution to (2.8) with the far-field condition (1.6) is found to be

$$\varphi_0(r,\bar{\mu}) = \left[\left(A_0 + \frac{B_0}{r}\right) + \left(A_1 r + \frac{B_1}{r^2}\right) P_1(\bar{\mu}) + \left(A_2 r^2 + \frac{B_2}{r^3}\right) P_2(\bar{\mu}) + \tfrac{1}{6}\bar{k}\sin(\bar{k}z_0) r^2\right] e^{it} \tag{2.9}$$

in which A_0, B_0, A_1, B_1, A_2 and B_2 are to be determined. Upon matching with the far-field potential φ_∞, we obtain

$$A_0 = \frac{1}{\bar{k}}\sin(\bar{k}z_0),$$

$$A_1 = \cos(\bar{k}z_0),$$

$$A_2 = -\tfrac{1}{3}\bar{k}\sin(\bar{k}z_0).$$

On the surface of the sphere, the normal velocity is taken to be zero because surface oscillations are neglected for the present range of interest. This gives

$$B_0 = -\tfrac{1}{3}\bar{k}\sin(\bar{k}z_0),$$

$$B_1 = \tfrac{1}{2}\cos(\bar{k}z_0),$$

$$B_2 = -\tfrac{2}{9}\bar{k}\sin(\bar{k}z_0).$$

Thus the expression for the potential φ_0 takes the form

$$\varphi_0 = \left\{\frac{1}{\bar{k}}\sin(\bar{k}z_0) + \cos(\bar{k}z_0)\left(r + \tfrac{1}{2}r^{-2}\right) P_1(\bar{\mu}) \right.$$
$$\left. - \tfrac{1}{3}\bar{k}\sin(\bar{k}z_0)\left[\left(r^{-1} + \tfrac{1}{2}r^2\right) + \left(r^2 + \tfrac{2}{3}r^{-3}\right) P_2(\bar{\mu})\right] + O(\bar{k}^2)\right\} e^{it}. \tag{2.10}$$

This result may be rigorously derived from the full solution of equation (2.7) in the form

$$\varphi_0(r, \bar{\mu}) = \sum_{n=0}^{2} \left[a_n j_n(\bar{k}r) + b_n y_n(\bar{k}r)\right] P_n(\bar{\mu}) e^{it}, \tag{2.11}$$

where $j_n(\bar{k}r)$ and $y_n(\bar{k}r)$ denote spherical Bessel functions, r is the dimensionless radial coordinate, and the angular eigenfunctions are limited to those in the far-field potential given in (1.6). Satisfying the zero normal velocity condition at $r = 1$ and satisfying (1.6) for the far-field by expansions in small $\bar{k}$ will yield a solution consistent with that from equation (2.8), that is, the above result (2.10).

The leading-order acoustic pressure p_0 and density ρ_0 are then given by

$$p_0 = \rho_0 = -\frac{\partial \varphi_0}{\partial t} = -i \left\{ \frac{1}{\bar{k}} \sin(\bar{k}z_0) + \cos(\bar{k}z_0) \left(r + \tfrac{1}{2} r^{-2}\right) P_1(\bar{\mu}) \right.$$
$$\left. -\tfrac{1}{3}\bar{k} \sin(\bar{k}z_0) \left[\left(r^{-1} + \tfrac{1}{2} r^2\right) + \left(r^2 + \tfrac{2}{3} r^{-3}\right) P_2(\bar{\mu})\right] O(\bar{k}^2) \right\} e^{it}. \tag{2.12}$$

2.1.2 *Liquid-phase region.* Before dealing with the gas-phase boundary layer we treat the liquid regions since this procedure turns out to be somewhat easier. Because the medium inside the sphere is a liquid, and the outside one is a gas, we may approximate the liquid motion as incompressible flow. Then the leading-order liquid flow satisfies

$$D^4 \hat{\psi}_0 = 0, \tag{2.13}$$

wherein D^2 is the operator

$$D^2 = \frac{\partial^2}{\partial r^2} + \frac{(1 - \bar{\mu}^2)}{r^2} \frac{\partial^2}{\partial \bar{\mu}^2}.$$

Equation (2.13) has the solution

$$\hat{\psi}_0 = \left[(\hat{A}_1 r^2 + \hat{B}_1 r^{-1})(1 - \bar{\mu}^2) + (\hat{A}_2 r^3 + \hat{B}_2 r^{-2}) \bar{\mu}(1 - \bar{\mu}^2)\right] e^{it}. \tag{2.14}$$

To satisfy the finite velocity condition at the origin, we require

$$\frac{1}{r^2} \hat{\psi}_0 < \infty,$$

from which we deduce that $\hat{B}_1 = \hat{B}_2 = 0$. On the surface of the sphere, the normal velocity is zero, and thus $\hat{A}_1 = \hat{A}_2 = 0$. As a result, we obtain

$$\hat{\psi}_0 = 0, \tag{2.15}$$

implying no flow at all to the leading order. This also means that the boundary layer, to this order, will satisfy the no-slip conditions as for a solid sphere.

2.1.3 *Gas-phase Stokes layer.* In the boundary layer, we express the velocity as

$$\boldsymbol{u}^b = u_r^b \hat{\boldsymbol{r}} + u_\theta^b \hat{\boldsymbol{\theta}}, \tag{2.16}$$

where u_r^b is the normal velocity, u_θ^b is the tangential velocity, and $(\hat{\boldsymbol{r}}, \hat{\boldsymbol{\theta}})$ are unit vectors. As we know, when $M^2 \gg 1$, the vorticity generated at the surface of the sphere is confined to a thin shear-wave layer of thickness $O(M^{-1})$ (see Riley (**21**)), and we can scale the normal velocity inside the shear-wave layer as

$$u_\eta^b = \frac{M}{\sqrt{2}} u_r^b. \tag{2.17}$$

Again, we seek a perturbation solution by expanding the velocity, the pressure and the density as powers of ε in forms similar to equations (2.1) to (2.3), that is,

$$\boldsymbol{u}^b = \boldsymbol{u}_0^b + \varepsilon \boldsymbol{u}_1^b + O(\varepsilon^2), \tag{2.18}$$

$$p^b = p_0^b + \varepsilon p_1^b + O(\varepsilon^2), \tag{2.19}$$

$$\rho^b = \rho_0^b + \varepsilon \rho_1^b + O(\varepsilon^2). \tag{2.20}$$

With the insertion of (2.18), (2.19) and (2.20) into the momentum equation (1.2), we have

$$\frac{\partial p_0^b}{\partial \eta} = 0 \tag{2.21}$$

and

$$\frac{\partial u_{\theta 0}^b}{\partial t} = -\frac{\partial p_0^b}{\partial \theta} + \frac{1}{2} \frac{\partial^2 u_{\theta 0}^b}{\partial \eta^2}, \tag{2.22}$$

where the inner variable η is defined as

$$\eta = \frac{M}{\sqrt{2}}(r - 1). \tag{2.23}$$

Equation (2.21) gives us the information that the leading-order pressure in the boundary layer is a function of θ and t only. Therefore, we have

$$p_0^b = p_0|_{r=1} = -i \left\{ \frac{1}{\bar{k}} \sin(\bar{k} z_0) + \tfrac{3}{2} \cos(\bar{k} z_0) P_1(\bar{\mu}) - \bar{k} \sin(\bar{k} z_0) \left[\tfrac{1}{2} + \tfrac{5}{9} P_2(\bar{\mu}) \right] \right\} e^{it}. \tag{2.24}$$

As discussed earlier, to leading order, the liquid phase has zero velocity. Therefore, the boundary condition at $r = 1$ is given by

$$u_{\theta 0}^b = 0 \quad \text{at } r = 1. \tag{2.25}$$

At the edge of the Stokes layer,

$$u_{\theta 0}^b \to \left. \frac{\partial \varphi_0}{\partial \theta} \right|_{r=1} \quad \text{as } \eta \to \infty, \tag{2.26}$$

and the solution of equation (2.22) with boundary conditions (2.25) and (2.26) is

$$u_{\theta 0}^b = \left\{ -\tfrac{3}{2} \cos(\bar{k} z_0) \sin\theta + \tfrac{5}{3} \bar{k} \sin(\bar{k} z_0) \sin\theta \cos\theta \right\} \left(1 - e^{-(1+i)\eta} \right) e^{it}. \tag{2.27}$$

Using the same scale as (2.17) in the continuity equation (1.1), we may deduce that

$$\bar{k}^2 \frac{\partial \rho_0^b}{\partial t} + \frac{\partial u_{\eta 0}^b}{\partial \eta} + \frac{1}{\sin\theta} \frac{\partial}{\partial \theta} \left(u_{\theta 0}^b \sin\theta \right) = 0. \tag{2.28}$$

Here, we assume the same adiabatic condition as the bulk of the fluid, that is, $\rho_0^b = p_0^b$, which is then given by (2.24). With the boundary condition $u_{\eta 0}^b = 0$ on the surface, the solution of $u_{\eta 0}^b$ is found to be

$$u_{\eta 0}^b = \left\{ 3\cos(\bar{k}z_0) \left[\eta - \tfrac{1}{2}(1-i)\left(1 - e^{-(1+i)\eta}\right)\right] P_1(\bar{\mu}) \right. \\ \left. - \bar{k}\sin(\bar{k}z_0)\left(\eta + \tfrac{10}{3}\left[\eta - \tfrac{1}{2}(1-i)\left(1-e^{-(1+i)\eta}\right)\right] P_2(\bar{\mu})\right)\right\} e^{it}. \tag{2.29}$$

Here, we notice that all the leading-order solutions, including velocity, pressure and density, are just the linear combination of two groups of results; one is when the sphere is placed at the velocity antinode, and the other one is at the node.

2.2 *First-order solutions*

As we are more interested in the steady streaming outside the sphere, we consider here only the steady-state components of the solutions. We begin with the boundary layer.

The continuity equation in the boundary layer to order ε becomes

$$\boldsymbol{\nabla} \cdot \boldsymbol{u}_1^b + \bar{k}^2 \langle \boldsymbol{\nabla} \cdot (\rho_0^b \boldsymbol{u}_0^b) \rangle = 0, \tag{2.30}$$

where $\langle\ \rangle$ denotes the time average over one wave cycle. As we already know the solutions of ρ_0^b and $\boldsymbol{u}_0^b$, we can show that

$$\langle \boldsymbol{\nabla} \cdot (\rho_0^b \boldsymbol{u}_0^b) \rangle = 0, \tag{2.31}$$

which implies that the first-order steady flow inside the boundary layer is incompressible. Equating terms to order ε in the momentum equation, we obtain

$$\frac{\partial p_1^b}{\partial \eta} = 0 \tag{2.32}$$

for the normal direction, and

$$\left\langle \rho_0^b \bar{k}^2 \frac{\partial u_{\theta 0}^b}{\partial t} \right\rangle + \left\langle u_{\eta 0}^b \frac{\partial u_{\theta 0}^b}{\partial \eta} \right\rangle + \left\langle u_{\theta 0}^b \frac{\partial u_{\theta 0}^b}{\partial \theta} \right\rangle = -\frac{\partial p_1^b}{\partial \theta} + \frac{1}{2}\frac{\partial^2 u_{\theta 1}^b}{\partial \eta^2} \tag{2.33}$$

for the tangential direction. Using the expression (2.27) for $u_{\theta 0}^b$ on the left-hand side of equation (2.33), and with equation (2.32) in mind, we may write (2.33) to $O(\bar{k})$ as

$$\frac{1}{2}\frac{\partial^3 u_{\theta 1}^b}{\partial \eta^3} = \frac{\partial}{\partial \eta}\left[\cos^2(\bar{k}z_0)\sin\theta\cos\theta\left\{\tfrac{9}{8}\left(1+e^{-2\eta}\right) - \tfrac{9}{4}e^{-\eta}\left[(\eta-1)\sin\eta + (\eta+1)\cos\eta\right]\right\}\right. \\ + \bar{k}\sin(\bar{k}z_0)\cos(\bar{k}z_0)\left\{\sin\theta\left[2 - \tfrac{1}{2}\eta e^{-\eta}(\sin\eta + \cos\eta)\right.\right. \\ + \tfrac{5}{4}\left(e^{-\eta}\sin\eta + e^{-2\eta}\right) - \tfrac{13}{4}e^{-\eta}\cos\eta\Big] + \sin\theta\cos^2\theta\left[-\tfrac{15}{4}\left(1+e^{-2\eta}\right)\right. \\ \left.\left.\left. + \tfrac{25}{4}e^{-\eta}(\eta\sin\eta + \eta\cos\eta - \sin\eta) + \tfrac{15}{2}e^{-\eta}\cos\eta\right]\right\}\Big]. \tag{2.34}$$

After successive integrations of (2.34), with the limit $u^b_{\theta 1} = o(\eta)$ as $\eta \to \infty$, we obtain

$$\begin{aligned} u^b_{\theta 1} = {} & \bar{k}\sin(\bar{k}z_0)\cos(\bar{k}z_0)\left\{\sin\theta\left[\tfrac{5}{8}e^{-2\eta} + \tfrac{5}{4}e^{-\eta}\cos\eta + \tfrac{17}{4}e^{-\eta}\sin\eta\right.\right. \\ & \left. + \tfrac{1}{2}\eta e^{-\eta}(\sin\eta - \cos\eta) + Q_1\right] + \sin\theta\cos^2\theta\left[-\tfrac{15}{8}e^{-2\eta}\right. \\ & \left.\left. - 20e^{-\eta}\sin\eta + \tfrac{25}{4}e^{-\eta}(\eta\cos\eta - \eta\sin\eta - \sin\eta) + Q_3\right]\right\} \\ & + \cos^2(\bar{k}z_0)\sin\theta\cos\theta\left\{\tfrac{9}{16}e^{-2\eta} + \tfrac{27}{4}e^{-\eta}\sin\eta\right. \\ & \left. + \tfrac{9}{4}e^{-\eta}(\eta\sin\eta - \eta\cos\eta + \cos\eta) + Q_2\right\} + O(\bar{k}^2), \end{aligned} \tag{2.35}$$

where Q_1, Q_2 and Q_3 are constants to be determined.

Inside the drop, assuming that the Reynolds number is small, the steady streaming satisfies Stokes equation, that is,

$$D^4\hat{\psi}_1 = 0. \tag{2.36}$$

Here, $\hat{\psi}_1$ is the stream function such that

$$\hat{u}_{r1} = \frac{1}{r^2\sin\theta}\frac{\partial\hat{\psi}_1}{\partial\theta}, \quad \hat{u}_{\theta 1} = -\frac{1}{r\sin\theta}\frac{\partial\hat{\psi}_1}{\partial r}.$$

We select a solution for $\hat{\psi}_1$ with a set of angular eigenfunctions consistent with the boundary-layer solution (2.35). In view of the boundary conditions

$$\frac{\hat{\psi}_1}{r^2} < \infty \quad \text{as } r \to 0 \text{ and } \hat{\psi}_1 = 0 \quad \text{at } r = 1 \tag{2.37}$$

the solution of equation (2.36) is of the form

$$\hat{\psi}_1 = F_1(r^2 - r^4)(1 - \bar{\mu}^2) + F_2(r^3 - r^5)\bar{\mu}(1 - \bar{\mu}^2) + F_3(r^4 - r^6)(5\bar{\mu}^2 - 1)(1 - \bar{\mu}^2). \tag{2.38}$$

Next, we apply the velocity and shear stress continuity conditions on the interface ($r = 1$), that is,

$$u^b_{\theta 1} = \hat{u}_{\theta 1} \quad \text{and} \quad \frac{M_\mu}{\sqrt{2}}\frac{\partial u^b_{\theta 1}}{\partial\eta} = \frac{\partial}{\partial r}\left(\frac{\hat{u}_{\theta 1}}{r}\right),$$

where $M_\mu = M\delta_\mu$ is the product of a large parameter, $M \gg 1$, and a parameter considered to be small, $\delta_\mu = \mu/\hat{\mu} \ll 1$; we treat M_μ as being of order unity.

After satisfying these conditions, we obtain the remaining constants and get the expressions for $u^b_{\theta 1}$ and $\hat{\psi}_1$ in (2.35) and (2.38). Thus

$$Q_1 = \tfrac{23}{168}\sqrt{2}M_\mu - \tfrac{15}{8}, \quad Q_2 = \tfrac{9}{80}\sqrt{2}M_\mu - \tfrac{45}{16} \quad \text{and} \quad Q_3 = -\tfrac{15}{56}\sqrt{2}M_\mu + \tfrac{65}{8}, \tag{2.39}$$

while the flow field inside the drop is given by

$$\begin{aligned} \hat{\psi}_1 = {} & \bar{k}\sin(\bar{k}z_0)\cos(\bar{k}z_0)\tfrac{1}{24}\sqrt{2}M_\mu(r^2 - r^4)(1 - \bar{\mu}^2) \\ & + \cos^2(\bar{k}z_0)\tfrac{9}{160}\sqrt{2}M_\mu(r^3 - r^5)\bar{\mu}(1 - \bar{\mu}^2) \\ & - \bar{k}\sin(\bar{k}z_0)\cos(\bar{k}z_0)\tfrac{3}{112}\sqrt{2}M_\mu(r^4 - r^6)(5\bar{\mu}^2 - 1)(1 - \bar{\mu}^2) + O(\bar{k}^2). \end{aligned} \tag{2.40}$$

It should be noted that this solution in the drop region is uniformly valid as there is no internal Stokes layer.

Since the steady flow in the boundary layer is incompressible, the stream function ψ_1^b can be introduced such that

$$u_{\eta 1}^b = \frac{1}{\sin\theta}\frac{\partial \psi_1^b}{\partial \theta} \quad \text{and} \quad u_{\theta 1}^b = -\frac{1}{\sin\theta}\frac{\partial \psi_1^b}{\partial \eta}. \tag{2.41}$$

Thus, using (2.35) in (2.41) and noting the constants in (2.39), the stream function in the boundary layer may be expressed as

$$\begin{aligned}\psi_1^b = -\Big\{ & \bar{k}\sin(\bar{k}z_0)\cos(\bar{k}z_0)\Big[\Big(-\tfrac{5}{16}e^{-2\eta} - 3e^{-\eta}\cos\eta - \tfrac{7}{4}e^{-\eta}\sin\eta \\ & - \tfrac{1}{2}\eta e^{-\eta}\sin\eta + \tfrac{23}{168}\sqrt{2}M_\mu\eta - \tfrac{15}{8}\eta + \tfrac{53}{16}\Big)(1-\bar{\mu}^2) \\ & + \Big(\tfrac{15}{16}e^{-2\eta} + \tfrac{65}{4}e^{-\eta}\cos\eta + 10e^{-\eta}\sin\eta \\ & + \tfrac{25}{4}\eta e^{-\eta}\sin\eta + \tfrac{65}{8}\eta - \tfrac{15}{56}\sqrt{2}M_\mu\eta - \tfrac{275}{16}\Big)\bar{\mu}^2(1-\bar{\mu}^2)\Big] \\ & + \cos^2(\bar{k}z_0)\Big(-\tfrac{9}{32}e^{-2\eta} - \tfrac{45}{8}e^{-\eta}\cos\eta - \tfrac{27}{8}e^{-\eta}\sin\eta - \tfrac{9}{4}\eta e^{-\eta}\sin\eta \\ & + \tfrac{9}{80}\sqrt{2}M_\mu\eta - \tfrac{45}{16}\eta + \tfrac{189}{32}\Big)\bar{\mu}(1-\bar{\mu}^2)\Big\} + O(\bar{k}^2).\end{aligned} \tag{2.42}$$

This inner solution is valid only in the shear-wave layer, and to complete the analysis we must also seek the steady streaming in the outer region, where

$$r - 1 = O(1).$$

The continuity equation outside the boundary layer to order ε becomes

$$\boldsymbol{\nabla}\cdot\boldsymbol{u}_1 + \bar{k}^2\langle\boldsymbol{\nabla}\cdot(\rho_0\boldsymbol{u}_0)\rangle = 0. \tag{2.43}$$

By inserting the expressions for ρ_0 and $\boldsymbol{u}_0$ here, we can show that $\langle\boldsymbol{\nabla}\cdot(\rho_0\boldsymbol{u}_0)\rangle$ is zero, and therefore

$$\boldsymbol{\nabla}\cdot\boldsymbol{u}_1 = 0. \tag{2.44}$$

This implies that the first-order steady flow outside the boundary layer is incompressible. Then, in a manner similar to the inner variable ψ_1^b, we introduce the outer stream function ψ_1 such that

$$u_{r1} = \frac{1}{r^2\sin\theta}\frac{\partial\psi_1}{\partial\theta}, \quad u_{\theta 1} = -\frac{1}{r\sin\theta}\frac{\partial\psi_1}{\partial r}. \tag{2.45}$$

In the limit of small streaming Reynolds number ($R_s \ll 1$) the outer streaming satisfies the Stokes equation

$$D^4\psi_1 = 0. \tag{2.46}$$

To obtain the solution to this equation, the angular eigenfunctions are chosen to be of the same form as the inner solution, ψ_1^b, given by (2.42). The far-field behaviour of the solution requires the flow velocity to decay away. At the surface we require matching with the Stokes-layer solution (2.42).

Thus, we obtain

$$\psi_1 = \bar{k}\sin(\bar{k}z_0)\cos(\bar{k}z_0)\left[\left(\tfrac{1}{8} - \tfrac{1}{24}\sqrt{2}M_\mu\right)\left(r - \frac{1}{r}\right)(1-\bar{\mu}^2)\right.$$
$$\left. - \left(\tfrac{13}{16} - \tfrac{3}{112}\sqrt{2}M_\mu\right)\left(\frac{1}{r} - \frac{1}{r^3}\right)(5\bar{\mu}^2 - 1)(1-\bar{\mu}^2)\right]$$
$$+ \cos^2(\bar{k}z_0)\left(\tfrac{45}{32} - \tfrac{9}{160}\sqrt{2}M_\mu\right)\left(1 - \frac{1}{r^2}\right)\bar{\mu}(1-\bar{\mu}^2) + O(\bar{k}^2). \qquad (2.47)$$

In summary, the internal circulation within the drop is defined by equation (2.40), while the steady streaming in the gas medium is given by (2.42) for the Stokes layer, and by (2.47) for the outer region. We note that the case of the solid sphere is recovered in all these expressions by letting the liquid-phase viscosity become large, that is, setting $M_\mu = 0$.

3. Discussion

In the above analysis, we find that the leading-order solution is a linear combination of the two groups of fundamental solutions corresponding to the sphere being placed at the node and antinode, respectively, of a standing wave. At higher orders, nonlinear effects become important and additional terms besides the two fundamental solutions are needed for the proper description of the flow. The result obtained for the solid sphere case is consistent with the outer solution of Lee and Wang (**11**) which allows for a slip velocity on the solid surface. In Figs 1 to 5, we plot the

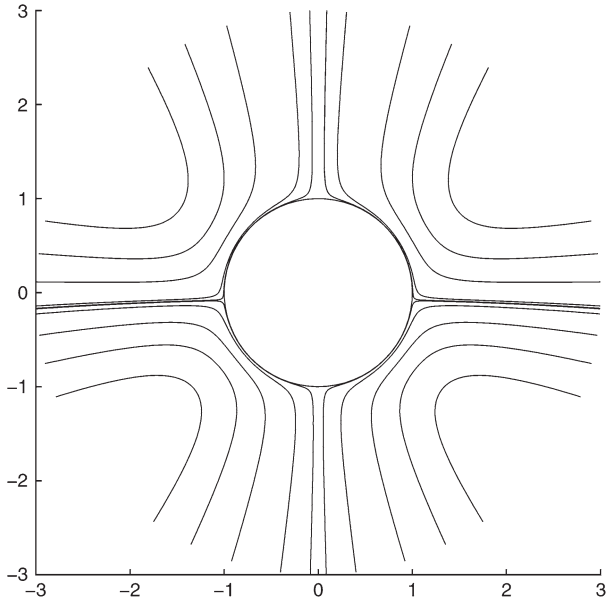

Fig. 1 Streaming about a solid sphere displaced between velocity node and antinode for $\bar{k}z_0 = \pi/8$, $\bar{k} = 0{\cdot}3$, and $M = 800$

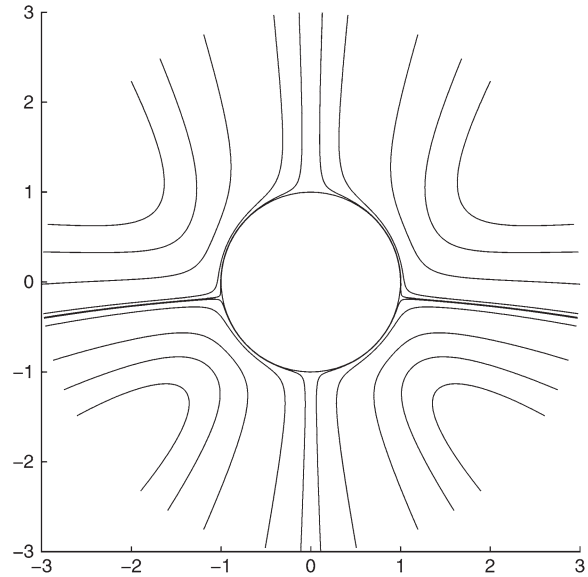

Fig. 2 Streaming about a solid sphere displaced between velocity node and antinode for $\bar{k}z_0 = \pi/4$, $\bar{k} = 0{\cdot}3$, and $M = 800$

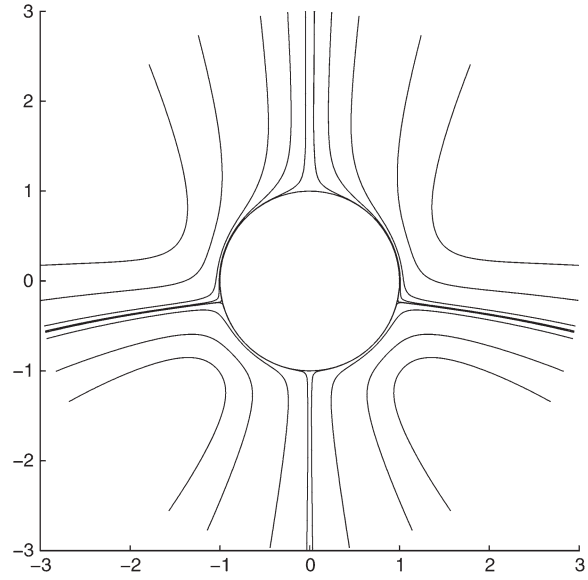

Fig. 3 Streaming about a solid sphere displaced between velocity node and antinode for $\bar{k}z_0 = 5\pi/16$, $\bar{k} = 0{\cdot}3$, and $M = 800$

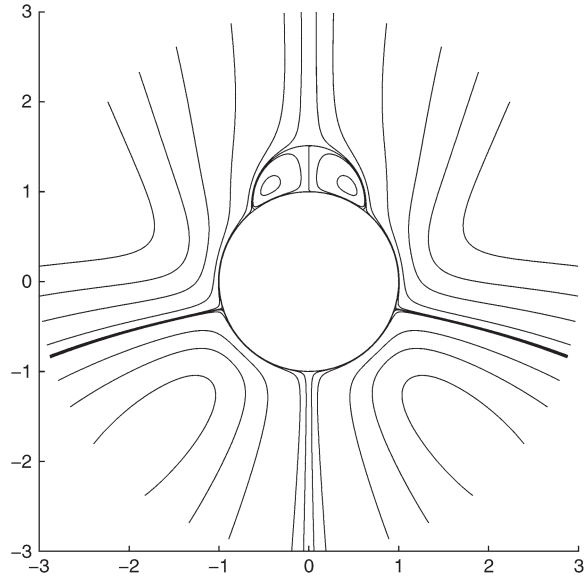

Fig. 4 Streaming about a solid sphere displaced between velocity node and antinode for $\bar{k}z_0 = 3\pi/8$, $\bar{k} = 0{\cdot}3$, and $M = 800$

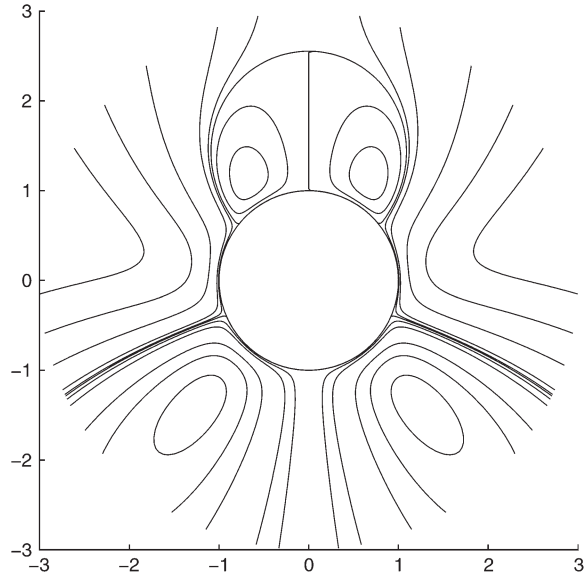

Fig. 5 Streaming about a solid sphere displaced between velocity node and antinode for $\bar{k}z_0 = 7\pi/16$, $\bar{k} = 0{\cdot}3$, and $M = 800$

streamlines for a solid sphere with $\bar{k} = 0{\cdot}3$. The asymmetry about the equator in the streaming pattern when the sphere is away from the velocity antinode is due to the asymmetric distribution of the undisturbed flow. The fluid velocity tends to be higher on the side of the velocity antinode, creating stronger streaming there. The flow pattern outside the sphere does not depend on M of course, but on the displacement $\bar{k}z_0$. There is a transition value in the flow pattern between $\bar{k}z_0 = 5\pi/16$ and $\bar{k}z_0 = 3\pi/8$. When $\bar{k}z_0$ is less than the transition value, there exists a thin recirculating region, limited to the Stokes layer adjacent to the surface, akin to that for a solid particle at the velocity antinode. This region is not clearly visible in Figs 1 to 3; however, when $\bar{k}z_0$ is larger than the transition value, larger vortices appear around the north-pole region as shown in Figs 4 and 5.

The leading-order oscillatory flow for a liquid sphere is essentially the same as for a solid one, in view of the high inertia of the liquid as compared to the surrounding gas medium. However, this is not the case for the steady streaming, when the difference between the liquid and the solid spheres may be appreciable. The effect of the 'liquidity' on the streaming is measured by the parameter M_μ. Typical flow patterns associated with the steady streaming of liquid sphere displaced between velocity node and antinode are displayed in Figs 6 to 13. In these figures, we plot the streamlines for $\bar{k} = 0{\cdot}3$, and $\bar{k}z_0 = \pi/4$. Equation (2.42) contains three terms that are linear in η, with coefficients a_1, a_2 and a_3, identified as

$$a_1 = \tfrac{23}{168}\sqrt{2}M_\mu - \tfrac{15}{8}, \tag{3.1}$$

$$a_2 = \tfrac{9}{80}\sqrt{2}M_\mu - \tfrac{45}{16} \tag{3.2}$$

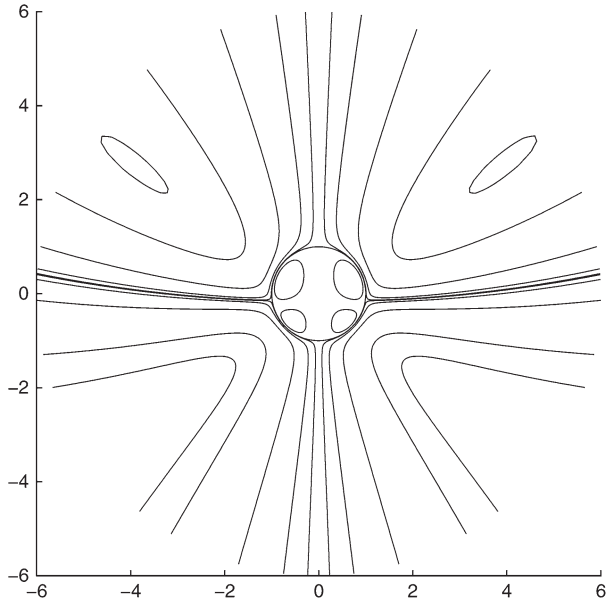

Fig. 6 Streaming about a drop displaced between velocity node and antinode for $\bar{k}z_0 = \pi/4$, $\bar{k} = 0{\cdot}3$, and $M_\mu = 3{\cdot}12$

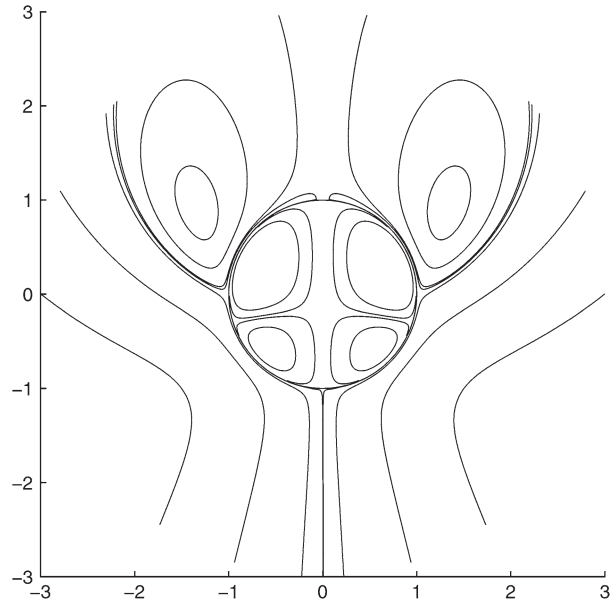

Fig. 7 Streaming about a drop displaced between velocity node and antinode for $\bar{k}z_0 = \pi/4$, $\bar{k} = 0{\cdot}3$, and $M_\mu = 9{\cdot}36$

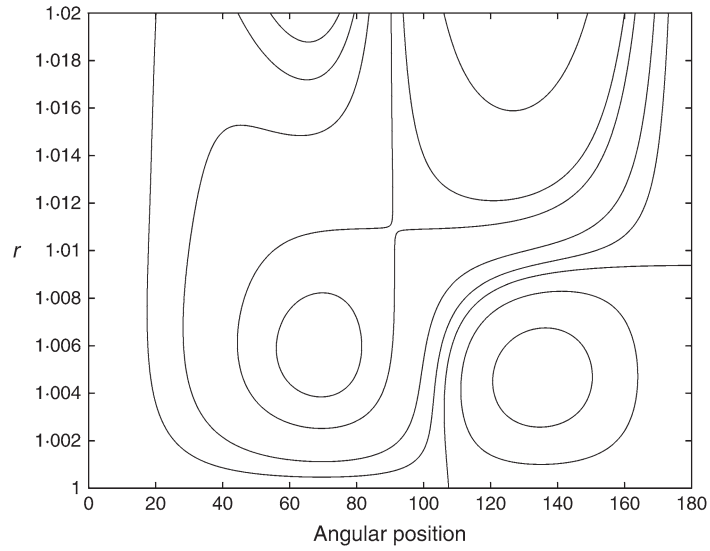

Fig. 8 Detailed streaming near the surface of drop stretched in the (θ, r)-plane for $\bar{k}z_0 = \pi/4$, $\bar{k} = 0{\cdot}3$, and $M_\mu = 9{\cdot}36$

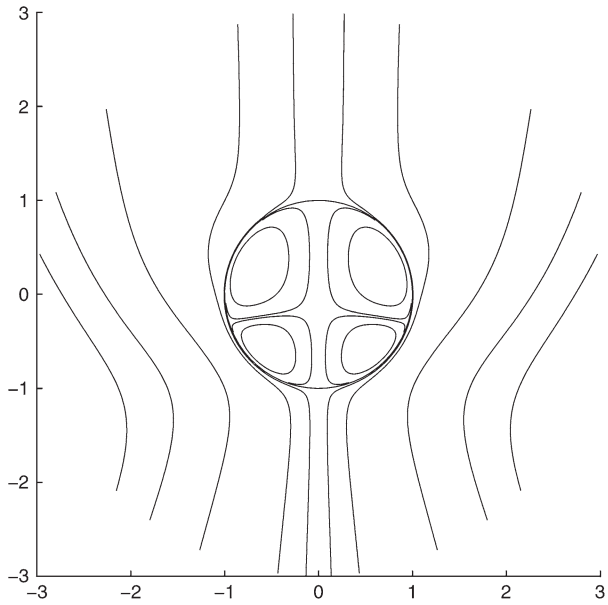

Fig. 9 Streaming about a drop displaced between velocity node and antinode for $\bar{k}z_0 = \pi/4$, $\bar{k} = 0{\cdot}3$, and $M_\mu = 12{\cdot}48$

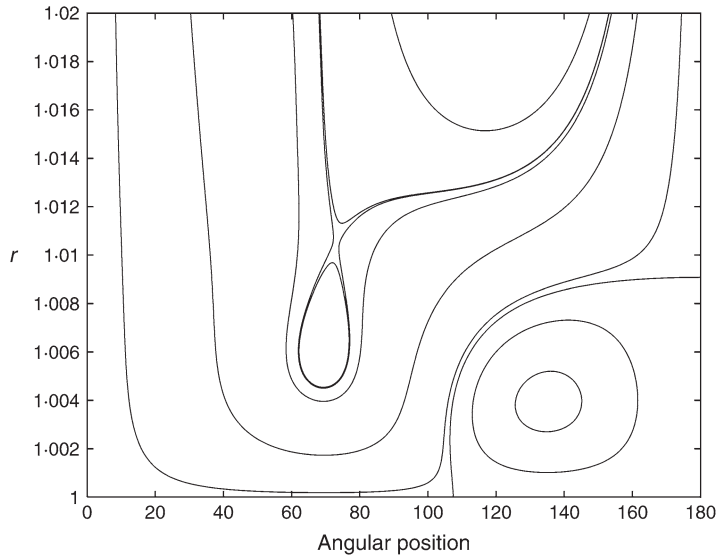

Fig. 10 Detailed streaming near the surface of drop stretched in the (θ, r)-plane for $\bar{k}z_0 = \pi/4$, $\bar{k} = 0{\cdot}3$, and $M_\mu = 12{\cdot}48$

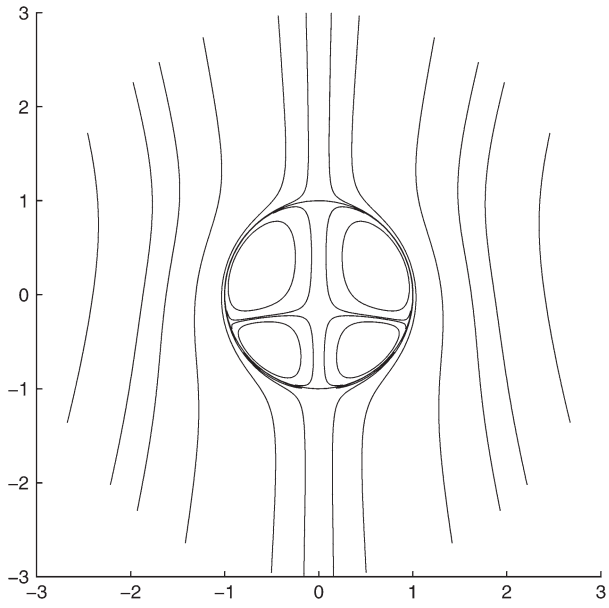

Fig. 11 Streaming about a drop displaced between velocity node and antinode for $\bar{k}z_0 = \pi/4$, $\bar{k} = 0{\cdot}3$, and $M_\mu = 19{\cdot}5$

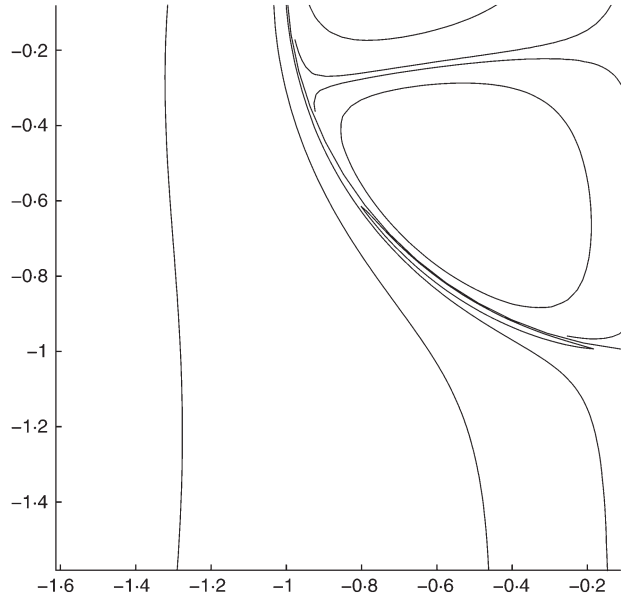

Fig. 12 Detailed streaming about the drop for $\bar{k}z_0 = \pi/4$, $\bar{k} = 0{\cdot}3$, and $M_\mu = 19{\cdot}5$

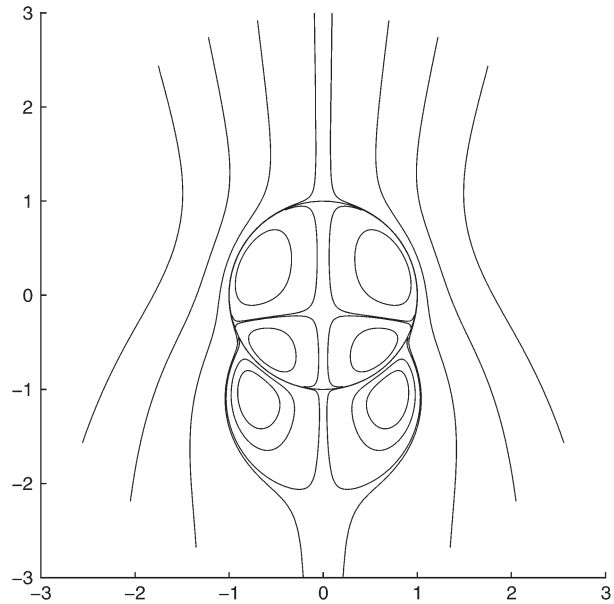

Fig. 13 Streaming about a drop displaced between velocity node and antinode for $\bar{k}z_0 = \pi/4$, $\bar{k} = 0{\cdot}3$, and $M_\mu = 28{\cdot}08$

and

$$a_3 = \tfrac{15}{56}\sqrt{2}M_\mu - \tfrac{65}{8}. \tag{3.3}$$

These three factors divide the range of M_μ into four smaller ones. Each of these is discussed next.

For

$$a_1 < 0 \quad \text{or} \quad M_\mu < \tfrac{315}{46}\sqrt{2},$$

there are vortices near the surface of the drop on the side of the velocity node, as shown in Figs 6 and 7. Here there is a large recirculatory region on the 'front side' of the drop with respect to the outer streaming which is downward. This may appear to be unusual from the standpoint of flows past obstacles that have a rear-side wake. However, with levitation, there is a low-pressure region on the top, and therefore it is possible for recirculation to occur in that region. An experimental result is shown in Fig. 14 which is qualitatively consistent with the theoretical prediction. While the experiment corresponds to $M = 113$, theoretical calculations at such a low value of M_μ do not show a 'front-side' recirculatory region. However, in the experiment, there are some effects such as those from the chamber walls that are not accounted for. There are a number of other interesting features in this flow field. There exist very thin recirculatory regions in the gas phase on the lower side of the drop. These are difficult to resolve graphically, except on a stretched scale (see Fig. 8). With an increase in M_μ, when

$$a_1 > 0 \quad \text{and} \quad a_2 < 0, \qquad \text{or} \qquad \tfrac{315}{46}\sqrt{2} < M_\mu < \tfrac{25}{2}\sqrt{2},$$

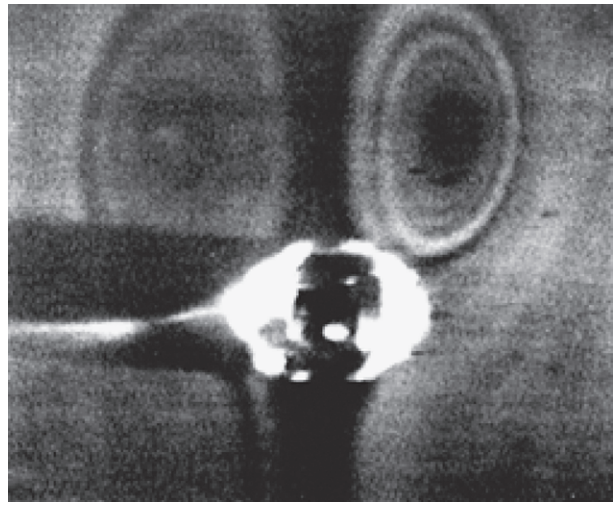

Fig. 14 An experimental result. The tested particle is a drop of water with diameter 1·8 to 1·85mm. The acoustic frequency is 37kHz, corresponding to $M \simeq 110$ and $M_\mu \simeq 2{\cdot}3$

the vortices disappear. While the streamlines inside the shear-wave layer join the outside ones smoothly, as shown in Fig. 9, the small recirculatory region still persists. With a further increase in M_μ, when

$$a_2 > 0 \quad \text{and} \quad a_3 < 0, \quad \text{or} \quad \tfrac{25}{2}\sqrt{2} < M_\mu < \tfrac{91}{6}\sqrt{2},$$

the thin layer of recirculation becomes apparent near the surface on the lower side of the drop, as shown in Figs 11 and 12. When M_μ is very large, corresponding to

$$a_3 > 0 \quad \text{or} \quad M_\mu > \tfrac{91}{6}\sqrt{2},$$

the thin layer of recirculation becomes enlarged and vortices are created on the side of the velocity antinode as shown in Fig. 13.

One of the important findings of the present study is the marked difference in the streaming flow behaviour about a liquid drop from that about a solid sphere, even when the liquid viscosity is quite high. It is apparent that the flow characterization is sensitive to surface mobility which affects the interaction of the acoustic wave with that surface. As shown by Schlichting (**15**) and by Riley (**21**), the interaction with a solid surface produces recirculating regions adjacent to the surface. However, as argued earlier by Zhao, Sadhal and Trinh (**29**), the flow behaviour resulting from vorticity generated at the interface by this interaction is affected by the surface mobility.

Acknowledgement

The support of this work by the US National Aeronautics and Space Administration under grant NAG8-1663 is gratefully acknowledged. The authors are very grateful to Professor Norman Riley (University of East Anglia) for valuable input.

References

1. L. V. King, On the acoustic radiation pressure on spheres, *Proc. R. Soc.* A **147** (1934) 212–240.
2. L. V. King, On the theory of the inertia and diffraction corrections for the Rayleigh disc, *ibid.* **153** (1935) 17–40.
3. R. E. Apfel, Technique for measuring the adiabatic compressibility, density, and sound speed of a submicroliter liquid sample, *J. Acoust. Soc. Amer.* **59** (1976) 339–343.
4. T. J. Asaki and P. L. Marston, Acoustic radiation force on a bubble driven above resonance, *ibid.* **96** (1994) 3096–3099.
5. A. I. Eller, Force on a bubble in a standing acoustic wave, *ibid.* **43** (1968) 170–171.
6. C. P. Lee and T. G. Wang, Acoustic radiation force on a bubble, *ibid.* **93** (1993) 1637–1640.
7. J. Wu and G. Du, Acoustic force on a small compressible sphere in a focused beam, *ibid.* **87** (1990) 997–1003.
8. K. Yosioka and Y. Kawasima, Acoustic radiation pressure on a compressible sphere, *Acoustica* **5** (1955) 167–173.
9. E. H. Trinh, Compact acoustic levitation device for studies in fluid dynamics and material science in the laboratory and microgravity, *Rev. Sci. Instrum.* **56** (1985) 2059–2065.
10. E. H. Trinh, Levitation studies of the physical properties and nucleation of undercooled liquids, *Proc. VII Euro. Symp. on Mat. and Fluid Sci. in Microgravity* Oxford, UK, September, 1989, volume ESA SP-295, January 1990.
11. C. P. Lee and T. G. Wang, Outer acoustic streaming, *J. Acoust. Soc. Amer.* **88** (1990) 2367–2375.
12. A. L. Yarin, B. Brenn, O. Kastner, D. Rensink and C. Tropea, Evaporation of acoustically levitated drops, *J. Fluid Mech.* **399** (1999) 151–204.
13. A. L. Yarin, M. Pfaffenlehner and C. Tropea, On the acoustic levitation of droplets, *ibid.* (1998) 65–91.
14. A. Rednikov and S. S. Sadhal, Steady streaming from an oblate spheroid due to vibrations along its axis, *ibid.* **499** (2004) 345–380.
15. H. Schlichting, Berechnung ebener periodischer Grenzchichtströmungen, *Physik Zeitschr.* **23** (1932) 327–335.
16. Lord Rayleigh, On the circulation of air observed in Kundt's tubes and some allied acoustical problems, *Phil. Trans. R. Soc.* A **175** (1883) 1–21.
17. W. L. Nyborg, *Physical Acoustics: Principles and Methods* (Academic Press, London 1965).
18. N. Riley, Oscillatory viscous flows: Review and extension, *J. Inst. Math. Appl.* **3** (1967) 419–434.
19. N. Riley, Acoustic streaming, *Encyclopedia of Acoustics* (ed. M. J. Crocker; Wiley, New York 1997) 321–327.
20. N. Riley, Steady streaming, *Ann. Rev. Fluid Mech.* **33** (2001) 43–65.
21. N. Riley, On a sphere oscillating in a viscous liquid, *Q. Jl Mech. Appl. Math.* **19** (1966) 461–472.
22. N. Riley, Streaming from a cylinder due to an acoustic source, *J. Fluid Mech.* **180** (1987) 319–326.
23. N. Riley, Acoustic streaming about a cylinder in orthogonal beams, *ibid.* **242** (1992) 387–394.
24. N. Riley and M. F. Wybrow, The flow induced by the torsional oscillations of an elliptic cylinder, *ibid.* **290** (1995) 279–298.
25. A. Gopinath, Steady streaming due to a small-amplitude torsional oscillations of a sphere in a viscous fluid, *Q. Jl Mech. Appl. Math.* **46** (1993) 501–520.

26. A. Gopinath, Steady streaming due to small-amplitude superposed oscillations of a sphere in a viscous fluid, *ibid.* **47** (1994) 461–480.
27. B. J. Davidson and N. Riley, Cavitation microstreaming, *J. Sound Vib.* **15** (1971) 217–233.
28. M. S. Longuet-Higgins, Viscous streaming from an oscillating spherical bubble, *Proc. R. Soc.* A **454** (1998) 725–742.
29. H. Zhao, S. S. Sadhal and E. H. Trinh, Internal circulation in a drop in an acoustic field, *J. Acoust. Soc. Amer.* **106** (1999) 3289–3295.
30. H. Zhao, S. S. Sadhal and E. H. Trinh, Singular perturbation analysis of an acoustically levitated sphere: Flow about the velocity node, *ibid.* **106** (1999) 589–595.